

Thermal management by manipulating electromagnetic parameters

Yun Wang(王云), Di-Fei Liang(梁迪飞), Tian-Cheng Han(韩天成), and Long-Jiang Deng(邓龙江)

Citation: Chin. Phys. B, 2024, 33 (**5**): 058403. DOI: 10.1088/1674-1056/ad34c6
Journal homepage: http://cpb.iphy.ac.cn; http://iopscience.iop.org/cpb

What follows is a list of articles you may be interested in

Adaptive genetic algorithm-based design of gamma-graphyne nanoribbon incorporating diamond-shaped segment with high thermoelectric conversion efficiency

Jingyuan Lu(陆静远), Chunfeng Cui(崔春凤), Tao Ouyang(欧阳滔), Jin Li(李金), Chaoyu He(何朝宇), Chao Tang(唐超), and Jianxin Zhong(钟建新)
Chin. Phys. B, 2023, 32 (**4**): 048401. DOI: 10.1088/1674-1056/acb768

Excellent thermoelectric performance predicted in Sb_2Te with natural superlattice structure

Pei Zhang(张培), Tao Ouyang(欧阳滔), Chao Tang(唐超), Chaoyu He(何朝宇), Jin Li(李金), Chunxiao Zhang(张春小), and Jianxin Zhong(钟建新)
Chin. Phys. B, 2021, 30 (**12**): 128401. DOI: 10.1088/1674-1056/ac012c

Fundamental and progress of Bi_2Te_3-based thermoelectric materials

Min Hong(洪敏), Zhi-Gang Chen(陈志刚), Jin Zou(邹进)
Chin. Phys. B, 2018, 27 (**4**): 048403. DOI: 10.1088/1674-1056/27/4/048403

Graphene-enhanced thermoelectric properties of p-type skutterudites

Dandan Qin(秦丹丹), Yuan Liu(刘嫄), Xianfu Meng(孟宪福), Bo Cui(崔博), Yaya Qi(祁亚亚), Wei Cai(蔡伟), Jiehe Sui(隋解和)
Chin. Phys. B, 2018, 27 (**4**): 048402. DOI: 10.1088/1674-1056/27/4/048402

Charge and spin-dependent thermal efficiency of polythiophene molecular junction in presence of dephasing

Z. Golsanamlou, M. Bagheri Tagani, H. Rahimpour Soleimani
Chin. Phys. B, 2015, 24 (**10**): 108402. DOI: 10.1088/1674-1056/24/10/108402

SPECIAL TOPIC — Heat conduction and its related interdisciplinary areas

Thermal management by manipulating electromagnetic parameters

Yun Wang(王云)[1,2], Di-Fei Liang(梁迪飞)[1,2,†], Tian-Cheng Han(韩天成)[1,2], and Long-Jiang Deng(邓龙江)[1,2]

[1] *National Engineering Research Center of Electromagnetic Radiation Control Materials, University of Electronic Science and Technology of China, Chengdu* 611731, *China*

[2] *Key Laboratory of Multi-spectral Absorbing Materials and Structures of Ministry of Education, University of Electronic Science and Technology of China, Chengdu* 611731, *China*

(Received 8 November 2023; revised manuscript received 4 January 2024; accepted manuscript online 18 March 2024)

Electromagnetic absorbing materials may convert electromagnetic energy into heat energy and dissipate it. However, in a high-power electromagnetic radiation environment, the temperature of the absorbing material rises significantly and even burns. It becomes critical to ensure electromagnetic absorption performance while minimizing temperature rise. Here, we systematically study the coupling mechanism between the electromagnetic field and the temperature field when the absorbing material is irradiated by electromagnetic waves. We find out the influence of the constitutive parameters of the absorbing materials (including uniform and non-uniform) on the temperature distribution. Finally, through a smart design, we achieve better absorption and lower temperature simultaneously. The accuracy of the model is affirmed as simulation results aligned with theoretical analysis. This work provides a new avenue to control the temperature distribution of absorbing materials.

Keywords: multi-physics field, electromagnetic–thermal coupling, microwave absorption, high power application

PACS: 84.60.Rb, 84.60.–h, 42.25.Bs, 91.60.Ki **DOI:** 10.1088/1674-1056/ad34c6

1. Introduction

Absorbing materials have widespread applications in radar, communication, stealth technology, and other fields. The absorbed electromagnetic wave energy will be converted into internal energy and distributed in the form of heat.[1] Recently, with the increasing use of high-power weapons and high-power antenna arrays, absorbers have been facing challenges when exposed to such high-power electromagnetic environments. These materials rise temperature swiftly in absorbing electromagnetic energy because of the low heat conductivity. The lack of power-handling capacity of wave-absorbing materials has become an essential factor restricting their development and application. Therefore, research on power-resistant absorbing materials has attracted intense attention because of their importance in guaranteeing the safety and dependability of military equipment and communication systems.

In recent years, researchers have mainly focused on two categories of electromagnetic–thermal coupling research. One is microwave heating technology,[2–4] which uses the energy absorbed from microwaves to generate and transfer thermal energy for specific applications. Prominent application scenarios include aircraft deicing,[5,6] medical microwave ablation therapy, microwave curing,[7–10] gas detection,[11–14] etc. The other is eliminating the effects of temperature rises resulting from the energy absorption, thereby improving the high-power processing capability of materials and enhancing their suitability for high-power applications.[15–17] The main technical methods for improving the thermal performance of wave-absorbing materials include forced heat dissipation, modifying the shape, adding vent holes, and embedding metal conductors. Gong *et al.*[18] found that heat dissipation performance and power handling density of materials may be significantly enhanced by properly planning vent holes and heat sink structures without deteriorating their absorbing capabilities. Chen *et al.*[19] explored the internal temperature variation of the polyurethane absorber under a continuous electric field by thermocouple testing and found that the slender pyramids can facilitate better heat transfer to the surroundings. Using electromagnetic–thermal coupling simulations, Chen *et al.*[20] confirmed that slender pyramids can enhance power handling capabilities. Then they investigated the effects of frequency and the distance between the antenna and the absorber tips on the temperature field at the same input power. The impact of these variables on the temperature field of the intricate structure, including the hollow pyramid absorber with ferrite tile, was also investigated by Adhyapak *et al.*[21] Additionally, using electromagnetic–thermal simulations, Jain *et al.*[22] investigated the impact of the shape of waveguide microwave loads on heat dissipation. Yin *et al.*[23] explored the impact of electromagnetic fields on the internal temperature field of silicon carbide pyramidal absorbers in unconventional environments. They also considered the influence of material conductivity changes on temperature and achieved bidirectional coupling between the electromagnetic field and the temperature field.

The above-mentioned works mainly report some thermal

[†]Corresponding author. E-mail: dfliang@uestc.edu.cn

© 2024 Chinese Physical Society and IOP Publishing Ltd

management techniques, the mechanism between electromagnetic parameters and the temperature field in absorbing materials remains unclear. In this paper, we systematically study the coupling mechanism between the electromagnetic field and the temperature field when the absorbing material is irradiated by electromagnetic waves. We find out the influence of the constitutive parameters of the absorbing materials (including uniform and non-uniform) on the temperature distribution. Based on our theory, a smart design is achieved with better absorption and lower temperature simultaneously. This work provides a better understanding of absorbing materials in terms of electromagnetic–thermal coupling and offers insights for potential optimizations in practical applications.

2. Electromagnetic–thermal coupling theory

The positive and negative charge centers within the material separate from each other when dielectric materials are exposed to electromagnetic fields, known as polarization. When the electromagnetic field changes, the electric dipole moment inside a material also changes; hence, the electric dipole moment oscillates in response to a periodically varied electromagnetic field. This oscillatory process results in friction and interactions between molecules and atoms, which leads to energy dissipation, with a part of the absorbed electromagnetic energy being converted into heat.[24] For dielectric materials with polarization losses, the complex permittivity is commonly used to illustrate their polarization properties, as demonstrated by

$$\varepsilon = \varepsilon' - \mathrm{j}\varepsilon'', \tag{1}$$

where ε' is the real part of the complex permittivity, ε'' is the imaginary part of the complex permittivity, which signifies its capacity to absorb electric field energy and convert it into heat.

The material will experience an increase in temperature as a result of the energy transforming from dielectric loss into internal energy. The electromagnetic thermal unidirectional coupling process is shown in Fig. 1(b). Therefore, this internal energy acts as the heat source in the temperature field of the material, following the heat conduction equation with an internal heat source when it reaches the steady state

$$\frac{\partial^2 T}{\partial x^2} + \frac{q_\mathrm{v}}{\lambda} = 0, \tag{2}$$

$$q_\mathrm{v} = \pi f \varepsilon'' |\boldsymbol{E}|^2, \tag{3}$$

where λ is the thermal conductivity of the material, f is the frequency, $\boldsymbol{E}$ is the electric field, and q_v respresents the average dielectric loss per unit volume, which can be obtained from the average Poynting vector, as shown in Eq. (3).

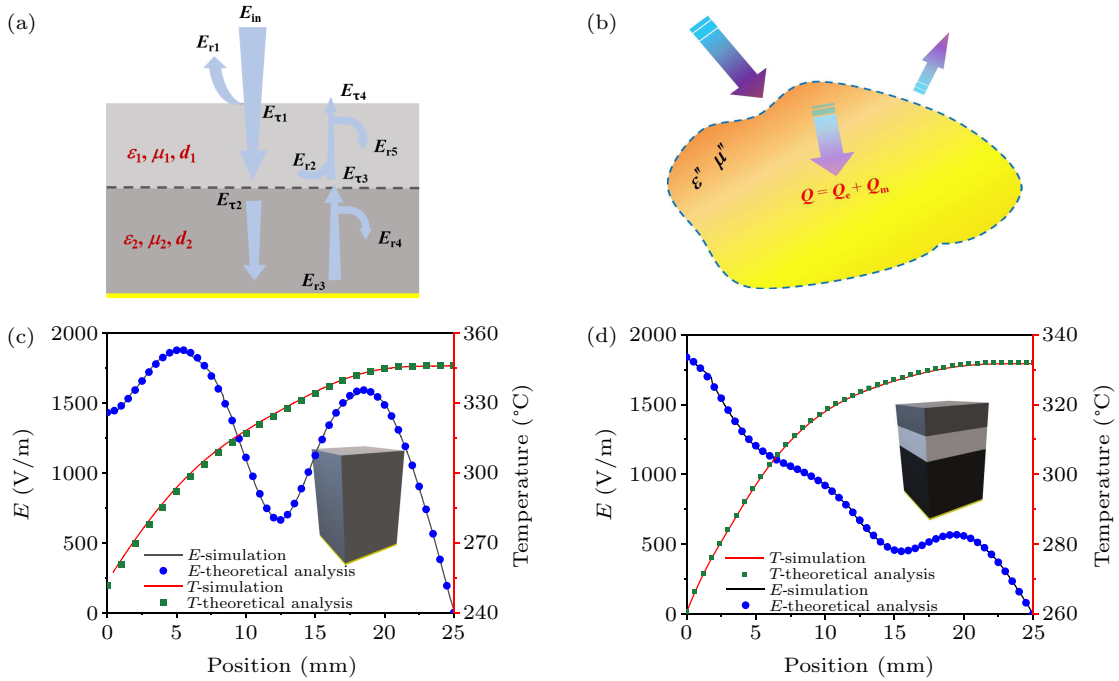


Fig. 1. Electromagnetic thermal coupling in materials. (a) Propagation path of electromagnetic wave in multilayer material. (b) Schematic diagram of electromagnetic–thermal coupling. (c) Theoretical analysis and simulation results of electric field and temperature distribution of the single-layer material. (d) Theoretical analysis and simulation results of electric field and temperature distribution of the multilayer material.

3. Results and discussion

We analyze the transmission characteristics and transmission path of the vertically incident electromagnetic wave inside the single-layer material. And then combine it with boundary conditions to get the rigorous solutions of the electromagnetic field and temperature field, as shown in Fig. 1(c). It is clear that the theoretical conclusions match with the simulation results, confirming the correctness of the whole ana-

lytical process. For the multi-layer dielectric loss material, a recursive algorithm is used to calculate the electric field distribution in the material. We considered the incident electromagnetic wave and its reflection and transmission process on material interfaces as a computational unit. Then, the reflected and transmitted electromagnetic waves on the material interface were respectively regarded as the incident waves for the new computational units and used to calculate the electric field in the next layer at their respective propagation directions. Based on the multiple refraction and reflection processes of electromagnetic waves in the multi-layer material, we iterated this recursive process until the electromagnetic wave attenuated to a very small value can effectively express the electric field distribution in the multi-layer lossy material. Subsequently, the distribution of power loss density was calculated using Eq. (3), and an approximate numerical solution for the temperature distribution was obtained. While each material layer had distinct ε'', resulting in a piecewise representation of power loss density in the multi-layer material, but the temperature distribution in the material still remained continuous. Thus, we considered the fact that the heat flux density should be continuous at the interface when the electromagnetic–thermal coupling process reaches a steady state and introduced interface continuity conditions to ensure continuity of the temperature. The following formula depicts the relationship at the layered interface:

$$\left(\lambda \frac{\partial T}{\partial x}\right)_i = \left(\lambda \frac{\partial T}{\partial x}\right)_{i+1}, \quad T_i = T_{i+1}, \tag{4}$$

where T_i represents the temperature of layer i, and T_{i+1} represents the temperature of layer $i+1$. The theoretical analysis results of electric field distribution and temperature distribution are shown in Fig. 1(d), which are also in great agreement with the simulation results and verify the accuracy of the model.

3.1. Single-layer homogeneous plate

Using the finite element approach, we simulated electromagnetic–thermal coupling on a single-layered plate with a height of 25 mm at 10 GHz, with an incident power density of 5 kW·m^{-2}. The perfect matching layer (PML) and scattering boundary condition were applied at the top in the setting of the electromagnetic field to simulate the open boundary to support the electromagnetic wave passing without reflection, minimizing the influence of reflected waves on the calculation domain. Periodic boundary conditions were applied on the sides of the sample to emulate an infinite-width plate. Heat dissipated from the upper surface through radiation and natural convection. The lower boundary is adiabatic, while the periodic boundaries on the sides of the sample are configured like the electromagnetic field setup.

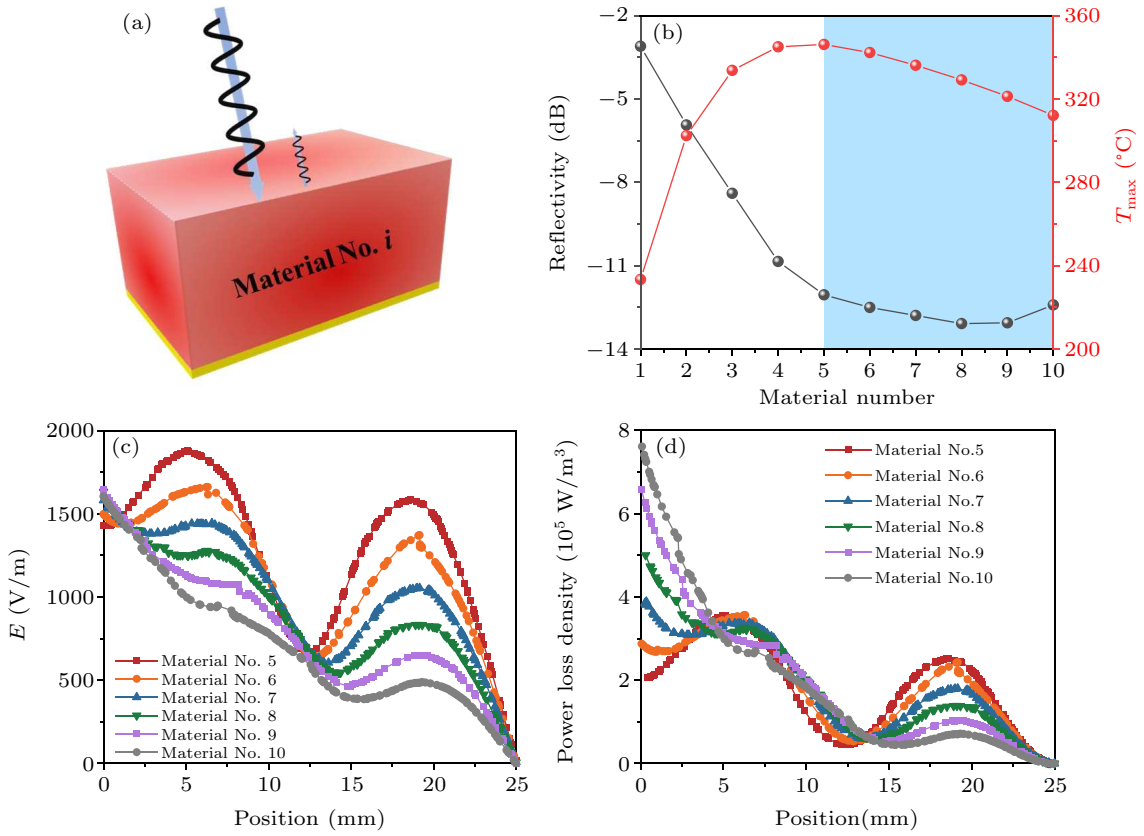


Fig. 2. Results of electromagnetic–thermal coupling of single-layer materials. (a) Schematic diagram of temperature rise of single layer absorbing material caused by electromagnetic wave irradiation. (b) Reflectivity and maximum internal temperature results of ten materials. (c) The electric field distribution of material No. 5 to material No. 10. (d) The power loss density distribution from material No. 5 to material No. 10.

Table 1. Parameters corresponding to each material number.

	No. 1	No. 2	No. 3	No. 4	No. 5
ε_r'	1.0716	1.1302	1.1926	1.2613	1.3383
ε_r''	0.0625	0.1233	0.1933	0.2720	0.3616
α	6.320	12.128	18.476	25.218	32.443
$\left\|\frac{Z_{in}}{Z_0}\right\|$	0.965	0.938	0.910	0.880	0.849
	No. 6	No. 7	No. 8	No. 9	No. 10
ε_r'	1.4255	1.5253	1.6394	1.7741	1.9359
ε_r''	0.4642	0.5827	0.7180	0.8808	1.0806
α	40.199	48.560	57.422	67.317	78.529
$\left\|\frac{Z_{in}}{Z_0}\right\|$	0.817	0.783	0.748	0.711	0.672

Firstly, the relationship between electromagnetic parameters and temperature for ten distinct materials was investigated in this paper. Table 1 lists the electromagnetic properties of each material, and Fig. 2(b) shows the associated reflectivity and the outcomes of simulated peak temperatures. As reflectivity decreases, materials No. 1 to No. 5 exhibit noticeably higher interior peak temperatures. This can be attributed to the decreased reflectivity resulting in greater absorption of electromagnetic energy and, consequently, more electromagnetic energy being converted into internal energy. In the case of materials No. 5 to No. 10, their reflectivity is around -12 dB. We calculate the matching constant and attenuation coefficient for each sample, as shown in Table 1. The attenuation constant (α) and the matching coefficient (Z)[25] are formulated as

$$\alpha = \omega\sqrt{\mu\varepsilon}\sqrt{\frac{1}{2}\left[\sqrt{1+\left(\frac{\varepsilon''}{\varepsilon'}\right)^2}-1\right]}, \tag{5}$$

$$Z = \left|\frac{Z_{in}}{Z_0}\right| = \left|\sqrt{\frac{\mu_r}{\varepsilon_r}}\tanh\left(\mathrm{j}\frac{2\pi f d}{c}\sqrt{\mu_r\varepsilon_r}\right)\right|, \tag{6}$$

where ω is the angular frequency, μ is the permeability, d is the thickness of the material, and c is the speed of electromagnetic waves in vacuum. Material No. 10 has a higher attenuation constant compared to material No. 5. However, material No. 10 has a lower matching coefficient, leading to a similar reflectivity as material No. 5. Consequently, both materials absorb a comparable quantity of electromagnetic energy. Additionally, we calculate the internal electromagnetic loss power for samples with dimensions of 10 mm $\times$ 10 mm $\times$ 25 mm. Materials No. 5 to No. 10 exhibit a total electromagnetic loss power of 0.47 W. This provides more evidence of the similarity in levels of absorbed electromagnetic energy. However, it is crucial to draw attention to the significant 34 °C temperature differential that exists among them. This difference implies that material No. 10 can withstand a higher incident power than material No. 5 under similar reflectivity. This is helpful for high-power applications requiring absorbing materials.

The maximum temperatures of material No. 5 to No. 10 differ noticeably when absorbing the same total electromagnetic energy. These disparities indicate the significant impact of electromagnetic parameter selection on electromagnetic–thermal coupling outcomes. To explain this phenomenon, the electric field distribution and power loss density distribution inside material No. 5 to No. 10 are analyzed, as shown in Figs. 2(c) and 2(d). It is clear that the attenuation rate of electromagnetic waves within the material progressively rises with the increase in electromagnetic characteristics of the material, aligning with the calculated results in Table 1. Based on the power loss density (q_v) equation, it is observable that the power loss density is directly correlated with the electric field E^2 and the dielectric loss factor ε''. Material No. 10 exhibits a higher ε'', resulting in a more concentrated power loss in the vicinity of its upper surface, coinciding with the heat dissipation boundary of the material coincidentally. As a consequence, the internal temperature of material No. 10 has the lowest value. Figures 3(a) and 3(b) depict the distribution of temperature, normalized electric field, and normalized power loss density for material No. 5 and material No. 10, respectively, in agreement with the findings.

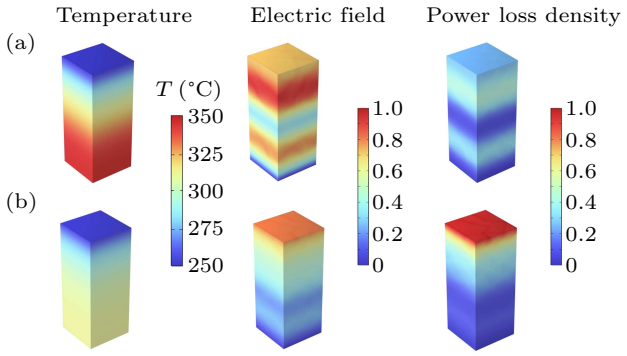


Fig. 3. Simulation results of temperature, electric field, and power loss density distribution. (a) Simulation results of material No. 5. (b) Simulation results of material No. 10.

In summary, the specific temperature distribution should be analyzed in combination with the power loss density distribution in the materials and the heat dissipation conditions. These results primarily highlight the electromagnetic parameter selection for wave-absorbing materials in the electromagnetic–thermal coupling process and provide data support for further optimizing the design and performance of absorbing materials.

3.2. Multilayer gradient design plate

Gradient design plays an essential role in significantly enhancing the absorption capability of the absorbing materials. Gradient design allows for better impedance matching when electromagnetic waves are incident, enabling as many electromagnetic waves as possible to enter the interior of the structure. The electromagnetic waves are absorbed after going through multiple reflections and refractions inside the material, minimizing the reflection of electromagnetic waves. Hence, combining with the aforementioned conclusion is best

to concentrate power losses close to the boundary of heat dissipation, gradient design presents an opportunity to enhance both wave absorption and temperature optimization.

The traditional approach in gradient design is progressively increasing the dielectric property of the material. However, this design strategy will make the high power loss density located far from the heat dissipation boundary, which hinders temperature optimization. Hence, we present a novel three-layer gradient design as illustrated in Fig. 4(a), accompanied by the corresponding results of the wave absorption effect and temperature distribution in Figs. 4(a) and 4(b). Evidently, the gradient design not only reduces the maximum internal temperature by 14.44 °C but also diminishes the reflectivity from −12.79 dB to −21.88 dB when compared to homogeneous material No. 5.

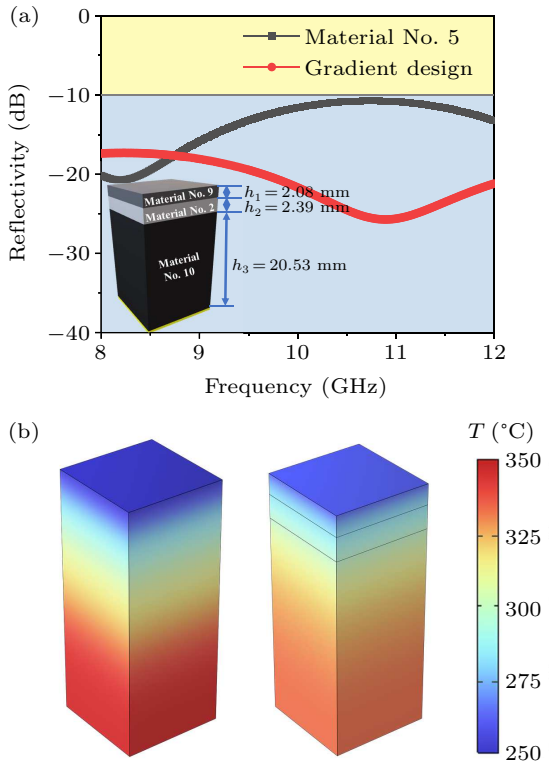


Fig. 4. Comparison of the single-layer material and gradient design structure. (a) Reflectivity results of material No. 5 and the gradient design structure. (b) Simulation results of temperature distribution of material No. 5 and the gradient design structure.

The calculated impedance matching coefficient for gradient design is 0.75, which is similar to uniform material No. 8. From Fig. 5(c), it can be observed that the electric field attenuation result of the gradient design is similar to that of material No. 9, indicating that the electric field attenuation result inside the gradient design is superior to material No. 8. Considering both the impedance matching and the electric field attenuation, the absorption performance of the gradient design is better than material No. 8 (−13.08 dB). Therefore, the absorption performance of the gradient design is better than materials from No. 5 to No. 10. Near the heat dissipation boundary, the electric field intensity of the gradient design is higher than material No. 5, which can be intuitively observed from the normalized electric field results of Figs. 5(a) and 5(b) as well as in Fig. 5(c). Furthermore, according to Eq. (3), the power loss density is proportional to $\varepsilon'' E^2$, and the upper material in the gradient design is selected as material No. 9, which also has a higher dielectric parameter. Therefore, the power density loss is mainly concentrated in the upper material, which is consistent with the result of normalized power loss density distribution in Fig. 5. The power loss mainly concentrating in the region close to the heat dissipation boundary is advantageous for heat dissipation. Consequently, the temperature is significantly reduced compared to that of material No. 5, aligning with the previous analysis.

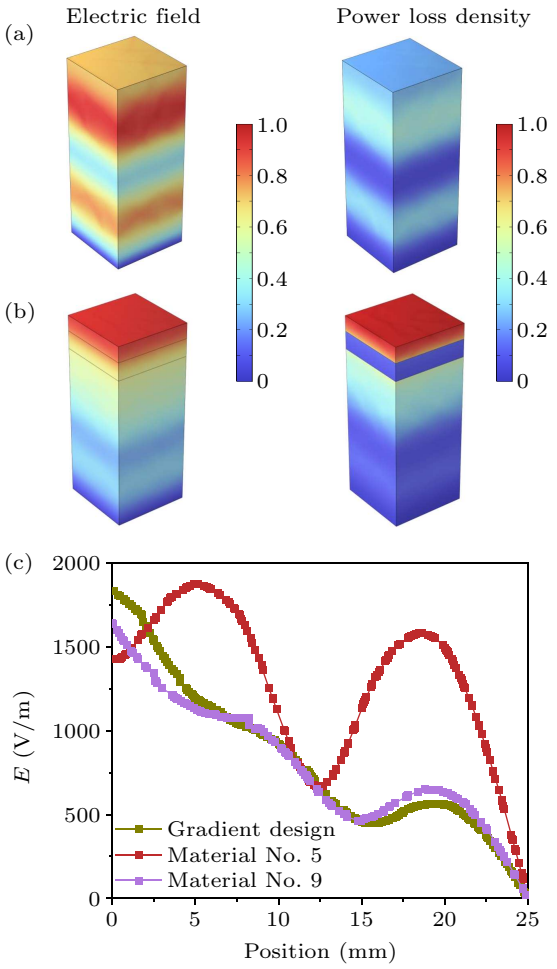


Fig. 5. The comparison results of the material No. 5 and the gradient design. (a) The results of normalized electric field and power loss density distribution for material No. 5. (b) The results of normalized electric field and power loss density distribution for gradient design. (c) The electric field attenuation results of gradient design and uniform materials.

More three-layer gradient design schemes are shown in Fig. 6(a), including the materials used for each gradient design and the corresponding thickness of each layer. Figure 6(b) shows the absorption performance and temperature results for each gradient design. To achieve better wave absorption performance and lower temperature than material No. 10, it may

be necessary to apply materials with higher dielectric parameters. Therefore, based on the ten materials given in the previous Subsection 3.1, the gradient results are compared with the results of uniform materials from No. 5 to No. 8.

From Fig. 6(b), it can be seen that the following six gradient designs all achieve optimization of both the wave absorption performance and thermal performance compared to the results of material No. 5 (−12.79 dB, 346.16 °C). In particular, gradient design 2 has lower reflectivity and lower temperature compared to material No. 8. The reflectivity result of gradient design 6 reaches −30.07 dB, and the temperature is still 4.22 °C lower than that of material No. 5. Similarly, the four-layer gradient design schemes and results are provided in Figs. 6(c) and 6(d), which also achieve both optimization of electromagnetic and thermal performance compared to material No. 5.

It can be clearly seen from Fig. 6(a) that under the boundary conditions in this paper, in order to achieve the simultaneous optimization of electromagnetic–thermal performance, the dielectric parameters of the materials should follow a three-level design concept of high–low–high. The top level should use materials with high dielectric parameters because the high power loss density at the heat dissipation boundary is conducive to temperature reduction. This layer should not be designed too thick; otherwise it will not be conducive to impedance matching. The main function of this thin layer is heat dissipate. The second level should use a material with smaller dielectric parameters; its role is mainly to carry out impedance matching to ensure that more electromagnetic waves enter the interior of the material. The third level should also be selected with higher dielectric parameters; the role of this layer is to ensure that the electromagnetic waves entering the interior of the material can be effectively attenuated.

This result suggests that structural design can achieve better absorption performance while maintaining a lower material temperature. In other words, the gradient-designed absorber can withstand higher incident power density without exceeding the safety temperature limits of the material. This holds significant advantages for high-power application scenarios.

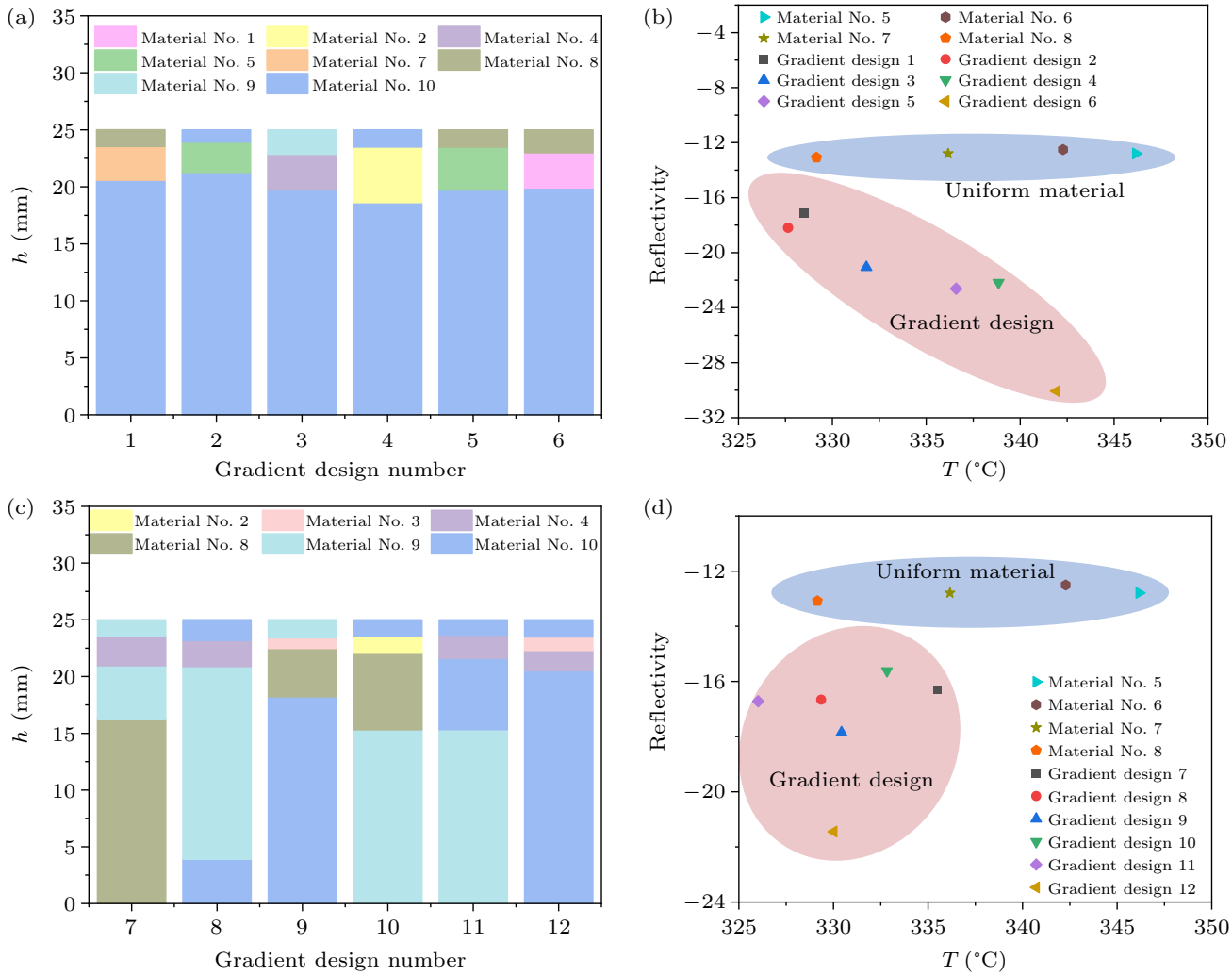


Fig. 6. The results of gradient designs. (a) The design scheme of three-layer gradient designs. (b) The absorption performance and temperature results of three-layer gradient designs. (c) The design scheme of four-layer gradient designs. (d) The absorption performance and temperature results of four-layer gradient designs.

4. Conclusion

Based on the multi-physical field analysis, rigorous solutions of the electromagnetic field and temperature field in the single-layer and multi-layer absorbing materials were obtained. These theoretical solutions were validated by aligning with simulation results, affirming the accuracy of our model. For single-layer absorbing material, it was found that there were notable temperature variations, even for materials with similar reflectivity. Areas of high power loss density within the material located at the heat dissipation boundary will benefit the internal temperature of the material. When analyzing the temperature distribution within materials, the power loss density distribution and the specific heat dissipation conditions should be considered simultaneously. In the case of multi-layer absorbing material, several gradient designs are given to optimize their electromagnetic–thermal performance simultaneously, and the gradient design strategy for the boundary conditions in this paper is summarized. This work serves as a reference for a better understanding of the electromagnetic–thermal coupling process and provides data support for electromagnetic–thermal balance design.

References

[1] Mo Z G 2019 *Research on Broadband Power-Resistant Absorbing Structure Based on FSS* (B.E. Dissertation) (Hunan: Hunan University of Science and Technology) (in Chinese)

[2] Chen Q, Chen X, Chen Z Z, Zhang B and Zheng Y Q 2019 *AIP Adv.* **9** 015113

[3] Tang L, Wang J, Zhang B, Li C and Jin H H 2022 *Compos. Sci. Technol.* **223** 109428

[4] Li Y G, Li N Y and Gao J 2014 *J. Adv. Manuf. Technol.* **70** 591

[5] Choi W H, Choe H S and Nam Y W 2020 *Compos. Part A Appl. Sci. Manuf.* **138** 106070

[6] Choe H S, Lee J S, Kweon J H, Nam Y W and Choi W H 2022 *Compos. Struct.* **283** 115138

[7] Walker J P, Swaminathan V, Haynes A S and Grebel H 2019 *Materials* **12** 2108

[8] Nuhiji B, Swait T, Bower M P, Green J E and Day R J 2019 *Compos. Part B Eng.* **163** 769

[9] Xu X H, Wang X Q, Wei R and Du S Y 2016 *Compos. Sci. Technol.* **123** 10

[10] Xu X H, Wang X Q, Liu W P, Zhang X, Li Z Z and Du S Y 2016 *Compos. Sci. Technol.* **97** 316

[11] Hong Y D, Lin B Q, Li H, Dai H M, Zhu C J and Yao H 2016 *Appl. Therm. Eng.* **93** 1145

[12] Lin B Q, Li H, Chen Z W, Zheng C S, Hong Y D and Wang Z 2017 *Appl. Therm. Eng.* **126** 949

[13] Huang J X, Xu G, Liang Y P, Hu G Z and Chang P 2020 *Fuel* **266** 117022

[14] Huang J X, Xu G, Hu G Z, Kizil M and Chen Z W 2018 *Fuel Process. Technol.* **177** 237

[15] Payne K, Xu K, Choi J H and Lee J K 2021 *IEEE Trans. Antennas Propag.* **69** 7624

[16] Payne K, Xu K, Choi J H and Lee J K 2018 *IEEE Trans. Plasma Sci.* **46** 934

[17] Wang C, Zhou J H, Zhou T, Chen Y L and Song H H 2019 *Mater. Rev.* **33** 84

[18] Gong P J, Liu L, Qi Y H, Yu W and Li F H 2017 *IEEE Trans. Electromagn. Compat.* **59** 1748

[19] Chen Z and Rodrigues V 2014 *IEEE Antennas Propag. Mag.* **56** 248

[20] Chen Z, Bayat H and Adhyapak A 2019 *Antenna Measurement Techniques Association Symposium*, October 6–11, 2019, San Diego, America, p. 1

[21] Adhyapak A and Chen Z 2020 *IEEE International Symposium on Electromagnetic Compatibility & Signal/Power Integrity*, July 28–August 28, 2020, America, p. 369

[22] Jain Y M, Dixit H V, Jadhav A R, Cheeran A N, Gupta V N and Sharma P K 2015 *IEEE Bombay Section Symposium*, September 10–11, 2015, Mumbai, India, p. 1

[23] Yin X F, Liu X N, Qin J Y and Du C L 2019 *IOP Conf. Ser.: Mater. Sci. Eng.* **608** 012009

[24] Mishra R R and Sharma A K 2016 *Compos. Part A Appl. Sci. Manuf.* **81** 78

[25] Fan B X, Xing L, Yang K X, Zhou F J, He Q M, Tong G X and Wu W H 2023 *Chem. Eng. J.* **451** 138492